DOI 10.1007/s10946-018-9756-7
Journal of Russian Laser Research, Volume 39, Number 6, November, 2018

USING LASER MEASURING AND SFM ALGORITHM FOR FAST 3D RECONSTRUCTION OF OBJECTS

Shuaihao Li, Yanxiang He, Qianqian Li, and Min Chen*

School of Computer Science, Wuhan University
Wuhan, China 430072

*Corresponding author e-mail: chenmin@whu.edu.cn

Abstract

Effective measurement of the reflective or transparent surface of an object has always been a disadvantage in laser scanning modeling. We propose a fast and complete three-dimensional (3D) reconstruction method for small static objects using laser scanning and the structure from motion (SFM) algorithm. Meanwhile, a complete reconstruction workflow is designed and a multi-angle 3d reconstruction system is set up. To generate the complete point cloud model of the object, the SFM algorithm is used to reconstruct the surface part of the object, the data for which cannot be obtained by the laser measuring instrument. The experimental results show that this method not only improves the speed, accuracy, integrity, and visual effect of 3D reconstruction of small objects, but also extends the scope of 3D reconstruction of laser measurement.

Keywords: laser measuring, rotating platform, SFM, 3D object reconstruction.

1. Introduction

In the 3D reconstruction of small static objects, the laser scanning measurement method [1] can directly acquire 3D information of the target surface and has higher reliability, However, it cannot efficiently express the texture feature of target surface, and it cannot effectively measure and obtain the data of the reflective and transparent parts of the surface. The SFM [2] algorithm for obtaining 3D coordinate data of objects from 2D image sequences is another 3D reconstruction method that is adopted to recover the external parameters of the camera and 3D information while the internal parameters of the camera are known. It can obtain the texture details of the object surface, but there are many problems, such as large calculation, low speed, low efficiency, and so on.

In this paper, we combine the laser scanner and the CCD camera to obtain point cloud data and RGB images from the 360° full vision of the small static object of the horizontal and vertical positions on the rotating platform. Then the point cloud model is generated by stitching the point clouds obtained, and the texture of the RGB image is mapped onto the corresponding point cloud model surface by image registration to generate a complete and real 3D object model. For the missing part of the model generated by laser measurement, the process of supplementing reconstruction using SFM algorithm is given. In the application of the SFM algorithm, we propose a method of 3D reconstruction, in which an image is taken every 5°, and an object has a total of 72×2 images from horizontal and vertical positions.

Manuscript submitted by the authors in English first on May 12, 2018 and in final form on June 08, 2018.

2. Laser Ranging and Two 3D Reconstruction Algorithms

2.1. The Laser Triangulation Ranging

The ranging methods of 3D laser scanning include pulse ranging, phase ranging, interference ranging, and triangulation ranging [3]. Among them, the triangulation ranging is simple in principle and structure of system components, high in measuring precision, low in hardware requirements, and extremely high in performance-price ratio. It is suitable for scanning measurement in medium and short distances. In this paper, the objects under study are close distance small objects, so triangulation ranging is adopted. It projects the laser onto the object to be measured to form a diffuse reflection, which is captured by the image acquisition module. The position coordinates of the point to be measured can be solved according to the position of the image acquisition module and the laser, and the geometric properties of the triangle and the imaging point information of the laser point in the image.

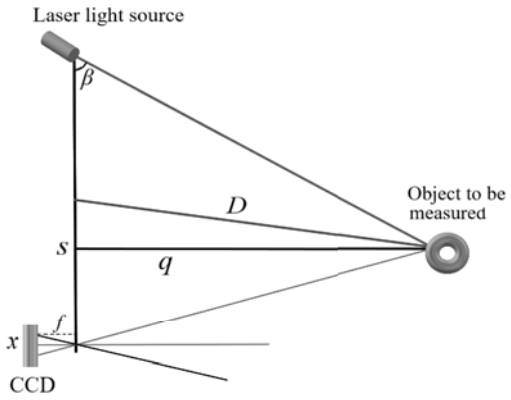

Fig. 1. Schematic of 3D laser triangulation ranging.

The working principle [4] is shown in Fig. 1.

The formula for solving the distance is as follows:

$$D = \sqrt{\left(\frac{fs}{p_x d_x + \Delta x}\right)^2 + \left[\frac{fs}{(p_x d_x + \Delta x)\sin\beta} - \frac{s}{2}\right]^2}. \quad (1)$$

Here, s is the distance between the CCD camera and the laser, x is the corresponding point of the laser spot in the image, f is the focal length of the CCD camera, and β is the angle between the laser and the line segment s. In addition, p_x is the horizontal coordinate of the pixels of the image point in the imaging plane, d_x is the unit size of the object corresponding to each pixel in the image, Δx is the deviation value, and D is the distance from the point at which the laser intersects with the object to the midpoint of s.

2.2. 3D Object Reconstruction Using Laser Measurements

The main processes of 3D object reconstruction using laser measurements are: the acquisition of point cloud data, point cloud pre-processing (error analysis and de-noising, etc.) [5], the registration, segmentation, and fusion of point cloud model, etc.

2.2.1. Point Cloud Registration

The point cloud data obtained by the laser scanner are partial point clouds at different angles, which need to be registered to the whole point cloud of object in the world coordinate system. To improve the efficiency of registration, the two transformation parameters – rotation matrix and the translation vector – are first solved, that is, the coarse registration is used to reduce the rotation and translational displacement between the point clouds. The registration error between two-point clouds is then minimized by accurate registration.

The scale-invariant feature transform (SIFT) algorithm [6] based on geometric features can effectively calculate the correspondence between point clouds, and the ICP algorithm [7] can acquire accurate

registration results. Therefore, in this paper, we use the SIFT algorithm as the coarse registration, and the ICP algorithm for accurate registration.

The ICP algorithm has been optimized by many researchers [8]. For example, the algorithm optimized by Rusinkiewicz is a fast convergence algorithm that applies various methods in different stages of the ICP algorithm and meets the requirement of real-time registration [9].

Jaesik Park et al. presented an algorithm for aligning two colored point clouds. The algorithm locks the alignment along both the normal direction and the tangent plane by optimizing a joint photometric and geometric objective. They extend a photometric objective for aligning RGB-D images to point clouds by locally parameterizing the point cloud with a virtual camera. The algorithm is more accurate and more robust than prior point cloud registration algorithms, including those that utilize color information [10].

2.2.2. Point Cloud Fusion

The registered multiple sub-point clouds need to be fused together to generate a new global point cloud model.

In this paper, we adopted a volume-based fusion method. Before the fusion process, a cube is defined in the world coordinate system, and the cube is segmented into many voxels according to a certain resolution. Then the truncated signed distance function (TSDF) [11] method is used to update the TSDF value of each small grid in the cube to restore the reconstruction model. Each voxel of TSDF stores the weighted symbolic distance function values and weights. The representation method based on distance function implicitly encodes the surface information into the data cube. The basic method of data fusion is to scan every voxel in the data cube.

The processing methods of scanning a single voxel (specify its coordinates as v_g) are as follows:

I. According to the transformation parameter $T = [R|t]$ of the current point cloud, it is transformed from the world coordinate to the camera coordinate,

$$v = R(v\_g - t). \tag{2}$$

II. To get the point P by perspective projection of v and calculate the value of SDF in the following way:

$$\mathrm{SDF} = \|t - v\_g\| - D(p). \tag{3}$$

III. If SDT≤ 0, the operation is exited; otherwise, the value of $\mathrm{TSDF}_i^{\mathrm{temp}}$ is calculated,

$$\mathrm{TSDF}_i^{\mathrm{temp}} = \min(1, \mathrm{SDF}/\mathrm{tran\_dist}). \tag{4}$$

IV. To calculate the new TSDF value and weight of voxel A and save it for the next scan to v_g,

$$w_i = \min(\max\_\mathrm{weight}, w_{i-1} + 1), \tag{5}$$

$$\mathrm{TSDF}_i = (\mathrm{TSDF}_i^{\mathrm{temp}} + \mathrm{TSDF}_{i-1})/(w_i + w_{i-1}). \tag{6}$$

2.3. Structure from Motion (SFM) Algorithm

We adopted the SFM method to recover the external parameters of the camera and 3D information while the internal parameters of the camera are known.

First, we obtained the basic matrix between two images by calculating the internal parameters of the camera and the feature point pairs between two images. Then the rotation matrix and translation

vector of the camera are obtained by the singular value decomposition of the essential matrix. Likewise, the 3D coordinates of each point in the image can be obtained by further subsequent calculations. After the above calculations, we obtain the sparse point cloud that is formed by all the feature points with 3D coordinates.

2.3.1. Feature Extraction and Matching

The SIFT algorithm is applied to detect, extract, and match the features of the preprocessed images. First, the difference of Gaussian (DOG) detection algorithm [12] is used to filter the images [13] and retrieve all the extreme points in the filtered image; then we extract the corresponding positions, scales, and rotation invariants and then match the features. Then the principal direction of the neighborhood gradient of the feature point is obtained as the direction of the feature point, so that the operator has rotation invariance and scale invariance.

The DOG formulas are as follows.

The one-dimensional formula reads

$$f(x;u,\sigma_1,\sigma_2)=\frac{1}{\sigma_1\sqrt{2\pi}}\exp\left[-\frac{(x-\mu)^2}{2\sigma_1^2}\right]-\frac{1}{\sigma_2\sqrt{2\pi}}\exp\left[-\frac{(x-\mu)^2}{2\sigma_2^2}\right]. \tag{7}$$

The two-dimensional formula is

$$f(u,v,\sigma)=\frac{1}{2\pi\sigma^2}\mathrm{e}^{-(u^2+v^2)/2\sigma^2}-\frac{1}{2\pi K^2\sigma^2}\mathrm{e}^{-(u^2+v^2)/2K^2\sigma^2}. \tag{8}$$

2.3.2. The Camera Calibration

To obtain the 3D coordinates of each point in the image, the internal and external parameters of the camera need to be solved, that is, the camera calibration. Camera calibration includes the self-calibration method based on image sequence [14] and the traditional method based on calibration object. Traditional calibration methods are complex and unsuitable for the situation without calibration object, but the accuracy of the self-calibration method is low. Noah et al. proposed to extract focal length information from the exchangeable image file (EXIF) and initialize the camera parameters by camera pose estimation. When the rough value of focal length is known, the bundle adjustment (BA) [15] method is used for nonlinear optimization of camera parameters, and the accurate values are further obtained.

For m-pair images containing n feature points, the solution of the objective function is

$$\min_{a_i,b_i}\sum_{i=1}^{n}\sum_{j=1}^{m}\theta_{ij}d[Q(a_j,b_i),x_{ij}], \tag{9}$$

where $Q(a_j,b_i)$ is the estimated projection matrix of point I on image j, x_{ij} is the coordinate of the ith projection point on the image j, and θ_{ij} is a coefficient. If the location of point i is on the image j, the value of θ_{ij} is 1; otherwise, it is zero. Recall that $\theta_{ij}d[Q(a_j,b_i),x_{ij}]$ is the Euclidean distance between $Q(a_j,b_i)$ and x_{ij}.

2.3.3. The Sparse Reconstruction

According to the camera internal parameters obtained by self-calibration, the essential matrix, the rotation matrix, and translation vector are further solved. Finally, the 3D coordinates of the spatial discrete points are calculated.

First, the basic matrix between two images is solved using the robust random sample consensus (RANSAC) algorithm. The corresponding points with dense matching points are randomly selected, and the basic matrix of multiple approximations is calculated using the normalized eight-point method. Then the approximate matrix with the highest accuracy of matching point pairs is selected as the final base matrix F [16]. Then the essential matrix E between two images, in which the internal reference matrix is known, respectively, K_1 and K_2, can be calculated by the formula below according to the basic matrix F between the two images

$$E = K_2^T F K_1. \tag{10}$$

The rotation matrix R and translation vector t of the camera are obtained by the singular value decomposition of the essential matrix E. Then the projection matrix corresponding to the two images is calculated using the rotation matrix R and the translation vector T. Likewise, the 3D coordinates of each point in the image can be obtained by further subsequent calculations. After the above calculations, we obtain the sparse point cloud that is formed by all the feature points with 3D coordinates.

Finally, the dense point cloud can be obtained by surface dense reconstruction of the sparse point cloud using the patch-based multi-view stereo (PMVS) algorithm proposed by Furukawa [17].

3. Design of 3D Reconstruction Workflow Based on Laser Measuring and SFM Algorithm

Since the laser measurement method is faster than the SFM algorithm in 3D reconstruction, the point cloud data is first used to reconstruct the object after the point cloud data and the RGB images are obtained. Then, the relevance feedback and integrity judgment of the reconstructed point cloud model are carried out. If there are missing parts on the model surface, the RGB images corresponding to the missing parts are retrieved, and the point cloud model of the missing part surface is generated by the SFM algorithm. Otherwise, the subsequent processes, such as mesh generation, surface rendering, and texture mapping, will be carried out to finally complete the 3D small static object reconstruction.

The complete workflow for 3D reconstruction of small static objects is shown in Fig. 2.

4. Data Acquisition and Coordinate System Setting

4.1. Collection of Point Cloud Data and RGB Images

The hardware system of 3D object reconstruction using laser measurement is composed mainly of the laser source, CCD camera, rotating platform, computer, and so on. Among them, the laser source is a 655 nm semiconductor laser [18] with a scanning accuracy of 0.03 mm. A linear structure laser is formed by the diffraction of a laser by a grating. A CCD camera fixed on the other side of the rotating rod is used to obtain a structured light stripe image is formed by the linear structure laser projected on a measured object. These images are used to extract the surface texture of the object by computer or to supplement

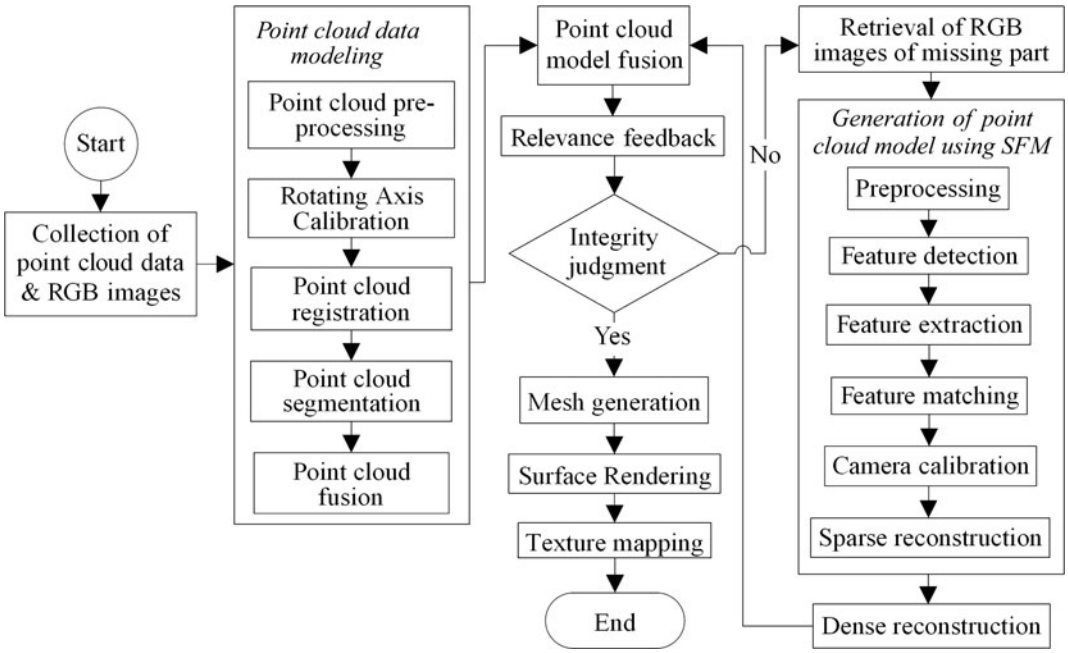

Fig. 2. The complete workflow for 3D reconstruction of small static objects.

reconstruction of the reflected or transparent surface by the SFM algorithm. The CCD camera is set to shoot continuously at a certain time interval. The speed is 3 images/s. The rotating platform can be accurately rotated around its central axis at a specified angle under computer control. In this study, we set the rotational speed of the rotating platform to 15° per second (equivalent to taking an image when the rotating platform rotates 5°). By placing the object to be measured vertically and horizontally on the rotating platform, data measurement and image acquisition of both horizontal and vertical positions are carried out. The laser and CCD camera, respectively, perform data scanning and RGB image acquisition of the small objects on the rotating platform and send them to the 3D reconstruction system in PC in real time. For the objects on the rotating platform, 360° full vision collection is performed from both horizontal and vertical positions, respectively. A total of $72 + 72$ images is collected for each object: one image is taken for each rotation of 5°.

4.2. Rotation Axis Calibration

The schematic of the measuring coordinates for data acquisition using the rotating platform is shown in Fig. 3. The left figure is the imaging process from point P in 3D space to 2D plane p.

Since the point coordinates of the objects calculated by stereo vision are in the camera coordinate system [19], in order to obtain the 3D coordinates of the objects in the turntable coordinate system, the relationship between the coordinate system of the turntable and the camera coordinate system needs to be calculated.

First, we carry out the rotation axis calibration [20,21]. The chessboard calibration board is placed on the turntable, and the images are taken at different rotation angles. According to the relationship between the rotation matrix and the right-hand coordinate system, given rotation axis $u = (u_x, u_y, u_z)(\|u\| = 1)$

and θ counterclockwise rotation angle, the rotation matrix is

$$R = I\cos\theta + \sin\theta[u]_x + (1-\cos\theta)u \otimes u, \tag{11}$$

where I is the unit matrix.

Then the rotation matrix R_y of the Y axis alignment and the rotation matrix R_x of the X axis alignment are calculated. Finally, the relationship between two coordinate systems can be obtained as the product $R_1 = R_x R_y$.

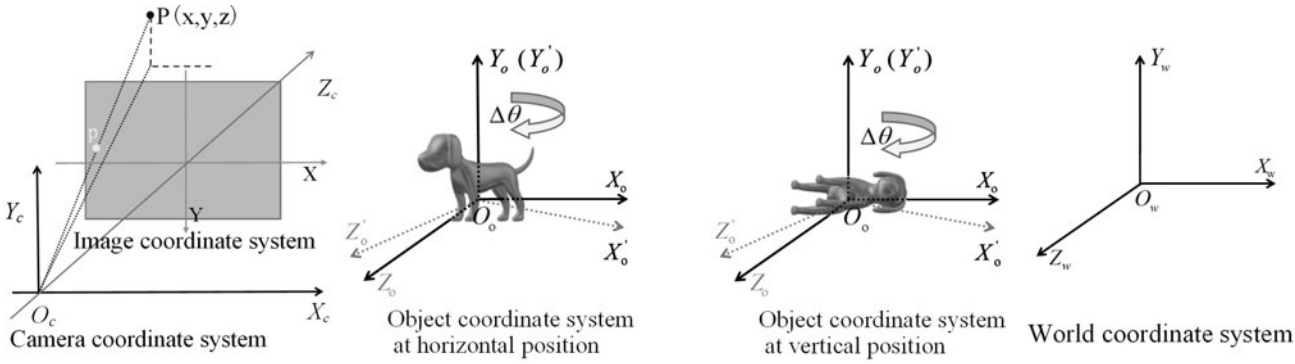

Fig. 3. The schematic of measuring coordinates of rotating platform.

The coordinates of objects in the camera coordinate system can be transformed into the rotating platform coordinate system by rotating and translating the matrix $R_1 R_t$.

According to formula (12), the rotation matrix R_2 of the object at different positions in the turntable coordinate system can be obtained. Finally, we obtain the equation of object coordinate transformation for different angles,

$$\begin{bmatrix} x_n \\ y_n \\ z_n \end{bmatrix} = R_2 \left(R_1 \begin{bmatrix} x \\ y \\ z \end{bmatrix} + T_1 \right), \tag{12}$$

where $x = [xyz]^T$ is the coordinates of the object at some angle in the camera coordinate system, and $x_n = [x_n y_n z_n]^T$ is the coordinate of the point after the turntable is rotated in the turntable coordinate system.

5. Experimental Results

Figure 4 shows the modeling of a glassware using the above processes and algorithms. The left figure is the point cloud generated by laser scanning. It shows that there are still missing parts on the surface of the generated point cloud model for the reflective position of the glass surface. The right figure shows the complete point cloud generated using the SFM algorithm after retrieving the RGB images corresponding to the missing parts surfaces. The results show that the 3D object reconstruction by combining laser scanning and the SFM algorithm is faster than that of the single SFM, while the integrity aspect is higher than that of single laser scanning.

6. Conclusions

Fig. 4. Comparison of point cloud integrity generated by two methods: laser scanning (on the left) and proposed algorithm (on the right).

We proposed a fast and complete 3D reconstruction method for small static objects using laser scanning method combined with the SFM algorithm. In the 3D reconstruction using laser scanning, the SFM algorithm is used to supplement the texture information of objects efficiently. This method solves the problem of insufficient integrity in single laser scanning reconstruction, and the speed is greatly improved compared with the single SFM algorithm. A complete reconstruction process is given and verified by experiments. The results show that the work flow and algorithm presented in this paper extend the scope of 3D reconstruction by laser measurement and have higher efficiency, accuracy, and integrity in 3D reconstruction of small static objects.

Of course, this method still has shortcomings. Although the method of laser scanning and photo data combination is a perspective approach for building textured 3D models, the method has some constraints; for example, it is barely usable for mirror and weakly scattering surfaces. In addition, the improvement is mainly reflected in the automation degree. First, the integrity judgment requires artificial participation. Second, the retrieval of RGB images corresponding to the missing part of the point cloud model depends on manual processing. To further enhance automation, the next work is to realize the automation of point cloud model integrity judgment by combining the RGB image and other factors, and thus to eliminate the process of relevant feedback. Furthermore, in the supplementary reconstruction, the research on RGB image automatic retrieval corresponding to the missing parts of the model could also be the focus of a follow-up study.

Acknowledgments

This study was funded by the Nature Science Foundation of China under Grants Nos. 91118003 and 61373039.

References

1. Q. B. Tong, B. Z. Han, D. L. Wang, et al., *J. Russ. Laser Res.*, **34**, 307 (2003).
2. M. A. Fonstad, J. T. Dietrich, B. C. Courville, et al., *Earth Surf. Process. Landforms*, **38**, 421 (2013).
3. L. Humbert, D. Hampf, P. Wagner, et al., *CEAS Space J.*, **8**, 1 (2015).
4. K. Konolige, J. Augenbraun, N. Donaldson, et al., "A low-cost laser distance sensor," contribution to the IEEE International Conference on Robotics and Automation, Washington (2008).
5. M. A. Selver, E. Y. Zoral, B. Belenlioglu, and Y. Soyaslan, "Interpolating and denoising point cloud data for computationally efficient environment modeling," contribution to the IEEE International Conference on Intelligent Rail Transportation, Birmingham (2016).
6. D. G. Lowe, *Int. J. Comput. Vis.*, **60**, 91 (2004).

7. M. Korn, M. Holzkothen, and J. Pauli, "Color supported generalized-ICP," contribution to the IEEE International Conference on Computer Vision Theory and Applications, New York (2015).
8. S. D. Billings, E. M. Boctor, and R. H. Taylor, *PloS One*, **10**, e0117688 (2015).
9. D. M. A. Latif, A. M. Salem, H. Ramadan, et al., "Comparison of 3D feature registration techniques for indoor mapping," *Int. Conf. Comput. Eng. Syst.*, **8255**, 239 (2013).
10. J. Park, Q. Y. Zhou, and V. Koltun, "Colored point cloud registration revisited," contribution to the IEEE International Conference on Computer Vision, IEEE Computer Society (2017), p. 143.
11. B. Curless and M. A. Levoy, "Volumetric method for building complex models from range images," contribution to the Conference on Computer Graphics and Interactive Techniques ACM, New York (1996).
12. P. S. Inn, B. Halil, H. Ding, et al., *PloS One*, **11**, e0157940 (2016).
13. C. Tomasi and R. Manduchi, "Bilateral filtering for gray and color images," *Proceedings of IEEE 6th International Conference on Computer Vision* (ICCV), New York (1998).
14. C. S. Fraser, *Photogram. Eng. Remote Sens.*, **79**, 381 (2013).
15. M. I. A. Lourakis and A. A. Argyros, *ACM Trans. Math. Software*, **36**, 1(2009).
16. R. I. Hartley, "In defense of the eight-point algorithm," *Proceedings of IEEE 8th International Conference on Computer Vision* (ICCV), **19**, 580(1997).
17. Y. Furukawa and J. Ponce, *IEEE Trans. Pattern Anal. Mach. Intell.*, **32**, 1362 (2010).
18. V. S. Gorelik, P. P. Sverbil', A. B. Fadyushin, et al., *J. Russ. Laser Res.*, **25**, 1 (2004).
19. N. Mellado, N. J. Mitra, and D. Aiger, *Comput. Graphics Forum*, **33**, 205 (2014).
20. J. Chen, L. Wang, Z. Liu, et al., *Microsyst. Technol.*, **23**, 3301 (2017).
21. H. Z. Li, H. L. Shen, and C. Cheng, *J. Comput. Applications*, **32**, 12 (2012).